Acta of Bioengineering and Biomechanics
Vol. 20, No. 2, 2018

Original paper
DOI: 10.5277/ABB-01080-2018-02

Three-dimensional biomechanical modeling and simulation of trephine cutting cornea for keratoplasty

PENG SU[1, 2], DA LU[1], SHIJING DENG[3], LEIYU ZHANG[4], YUXIN HAO[1], YANG YANG[5]*

[1] School of Electromechanical Engineering, Beijing Information Science and Technology University, Beijing, China.
[2] Key Laboratory of Rehabilitation Aids Technology and System of the Ministry of Civil Affairs, National Research Center for Rehabilitation Technical Aids, Beijing, China.
[3] Beijing Institute of Ophthalmology, Beijing Tongren Eye Center, Capital Medical University, Beijing, China.
[4] College of Mechanical Engineering and Applied Electronics Technology, Beijing University of Technology, Beijing, China.
[5] School of Mechanical Engineering and Automation, Beihang University, Beijing, China.

Purpose: Trephination is one of the basic operations of keratoplasty, and the biomechanical mechanism of the operation can be revealed based on three-dimensional modeling and simulation of trephine cutting cornea. *Methods:* Based on the analysis of the physical and biomechanical characteristics of corneal trephination, a three-dimensional numerical model of corneal trephination is built, where the cornea can be simplified to two layers structure including stroma and epithelium, and the trephine cuts the cornea under the vertical motion load and the rotational motion load. A three-dimensional failure criterion of corneal material is proposed based on the yield strength theory. On this basis, trephination simulation is carried out, and the units of corneal material are removed from the model when they meet the defined failure criterion. *Results*: Under the given parameters including the velocity, the angle and the angular velocity, the trephine force curves, include the linear cutting force and the rotary cutting force are obtained, and show the change of the forces with displacement during the process of trephination simulation. The maps of the equivalent stress show the destruction and deformation of the cornea. Then, the experiment of robotic trephination is carried out under the same parameters and the effectiveness of the simulation is evaluated. *Conclusions*: Based on mechanics theory and finite element method, the process of trephine cutting cornea has been reproduced, and the interaction mechanism is revealed, which lays the foundation for the development of real-time simulation and virtual system of the corneal surgery.

Key words: *cornea, trephine, biomechanics, failure criterion, finite element simulation*

1. Introduction

Keratoplasty as a delicate microsurgical surgery is using the healthy corneal graft to replace lesion part of the cornea in order to achieve the purpose of improving vision or treating corneal diseases. The surgical procedures can be divided into three steps, i.e., trephination, transplantation, and suture. Among them, trephination is the most basic operation in making corneal bed and graft in keratoplasty, which plays an important role.

Nowadays, some surgical procedures for trephination are manual operations. The manual operations have the advantages of controllability, simple operation and low-cost, but the effect of the operations depends on experience of surgeon and technology used and is limited by physiological limitations of surgeon. Particularly, manual operation will lead to a loss of endothelial cells at the cutting edge [5], [22], and it leads to non-uniform cutting force, and irregular graft or bed, which induces postoperative astigmatism and complications [2], [9]. Because of this, the researchers evaluated the effects of various trephination instruments and methods on the surgery [12], and explored the use of advanced technologies, such as robotics technology, laser technology and so on [12], [14], [27].

* Corresponding author: Yang Yang, School of Mechanical Engineering and Automation, Beihang University, XueYuan Road No. 37, HaiDian District, Beijing 100191, China. Phone: +86 01082339698, e-mail: yang_mech@126.com

Received: January 5th, 2018
Accepted for publication: March 19th, 2018

Robot-assisted keratoplasty is a surgical procedure that is similar to the traditional manual operation, and it has the advantages of stable operation and high reliability. Based on the signals from micro-force sensor and position sensor, the robot manipulator of trephination can judge the organizational state information and cutting depth, which can effectively improve the cutting precision and make up for the shortcomings of manual operation [14], [27]. In the field of surgery, many scholars are also exploring the trephination robot which has the ability to interact with biological tissues in real-time [10], [26]. In addition, laser technologies are also increasingly used in resecting corneal lesion and making corneal grafts, such as the excimer laser technology, the femtosecond laser technology and so on [25], [29]. As a new technology, the femtosecond laser technology has many advantages over traditional corneal surgery, such as accurate control of the cutting depth and corneal shape, and higher verticality in the edge of the cornea [15]. The study found that the open eyes and corrected visual acuity were significantly improved after surgery. Although the surgery is better using femtosecond lasers, the technology still has many problems and limitations, such as insecurity, instability, limitations, economic factors or other issues [22], [25].

With the development and progress of medical technology, in addition to improving surgical techniques and developing surgical manipulator, we should also make clear the biomechanical mechanism of the surgery [18]. The surgical mechanism can reveal interaction of instruments with tissue radically and be used to guide the design of the surgical manipulator [4]. Some researchers simulated the biomechanical deformation of corneal tissue using the finite element method, and simulated the damaged mechanism of the tissues of the eyeball in the case of external force acting on the eyeball [11], [28]. In addition, the finite element simulation on interaction of instruments with tissue can be using to the development of virtual surgery training system, and the numerical simulation can not only be used as a tool for surgical planning, evaluation and judgment of the operation, but also establish the mechanical condition that cannot be achieved in experiments [17], [21].

Because the cornea is a complicated viscoelastic body, there are many difficulties in researching interaction mechanism of instruments with corneal tissue, including the deformation of biological tissues in loading, the relaxation effects of tissue penetration, and simulation setting in numerical simulation. In the preliminary study, a corneal suture test system was built and the biomechanical model of needle insertion into cornea was established, and the biomechanical characteristics of was analyzed based on insertion experiment and finite element simulation [29]. In most of the simulation on the interaction of the instruments with biological soft tissue, such as insertion simulation [6], [17], [24], the soft tissue is simplified to be a two-dimensional model. Horever, the surgery of corneal trephination has a more complex biomechanical behavior, and some parameters may influence the results including linear velocity, rotation angle and rotation velocity [22]. It is necessary to establish a three-dimensional numerical model of trephination in order to reveal the biomechanical response of the operation effectively.

The interaction mechanism between trephine and the corneal tissue should be discussed due to the importance of corneal transplantation. The finite element model of corneal trephination is established based on the operation, and the failure criterion of corneal material is derived using the fourth strength theory. On this basis, three-dimensional biomechanical simulation on interaction of trephine with corneal tissue is performed, and the effectiveness of the simulation is evaluated through comparing cutting force curves with robotic experiment and analyzing the maps of equivalent stress.

2. Materials and methods

2.1. Finite element modeling of corneal trephination

Considering the operation requirements and characteristics of finite element simulation, geometric model of eyeball is built according to the physiological structure [11], [13], as shown in Fig. 1a. In the trephination experiment, disposable corneal trephine of 7.5 mm diameter was chosen [22], and its geometric model is shown in Fig. 1b.

According to the structure and biomechanical properties of the cornea, the cornea can be divided into five layers, including epithelium, lamina elastica anterior, stroma, lamina elastica posterior, and endothelium, and they have different geometric thickness and different mechanical properties, such as elastic modulus and Poisson's ratio. But in a lot of research on corneal mechanical behavior under different loads the cornea is simplified as the biological soft tissue that has only one layer structure [20]. In the cornea surgical operation, the mechanical response caused by interaction of

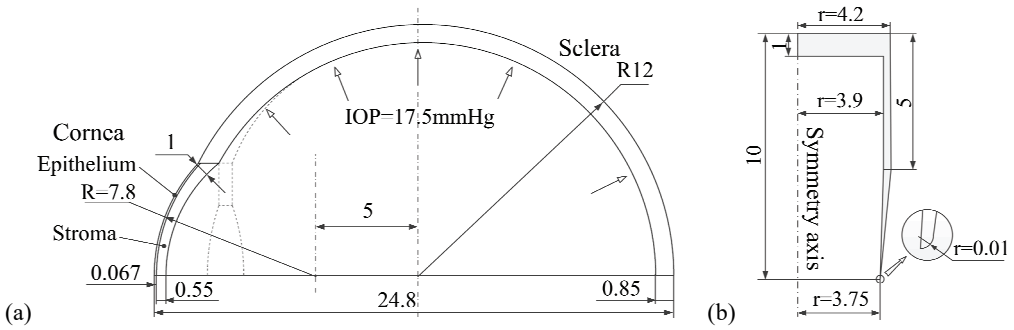

Fig. 1. The geometric model (dimension are given in mm).
(a) geometric model of eyeball, (b) geometric model of trephine

rigid instrument and flexible corneal tissue can be used as a reference for accurate control of the cutting depth [1], so the model of corneal trephination is established considering the different corneal layers. The stroma constitutes about 90% of corneal thickness, which is the main part of the cornea and determines biomechanical properties of the cornea. Epithelium, the second thickest layer of the cornea, is generally considered to be a corneal barrier because it is hard and located at the outwards. The other layers are so thin that they may be ignored in finite element simulation of corneal trephination, so in order to reduce the difficulty of calculation, the cornea is simplified to two layers structure, including stroma and epithelium, as shown in Fig. 1a. Mooney–Rivlin hyperelastic material parameters of stroma and neo-Hookean hyperelastic material parameters of epithelium are set up in the simulation model [13], [23], and the sclera was simplified as an elastic body that the elastic modulus $E = 3.08$ MPa and Poisson's ratio $\mu = 0.49$ [3].

In the process of cutting the corneal tissue with a trephine, there is vertical and rotational movement. Three-dimensional finite element model of trephine cutting cornea is established as shown in Fig. 2. In the model, the difference between vertical and horizontal of eye model is ignored, and the eyeball model and the trephine model are established by the method including 3D, deformable, solid, and rotation. For observation and analysis, the rotation angle of the cornea is 180 degrees, and the rotation angle of the trephine is 360 degrees. Based on the physiological structure of the eyeball, the sclera and cornea are used as the whole, and the biomechanical response of other eyeball tissues such as the choroid and the retina are ignored in the finite element analysis. The intraocular pressure is produced by chamber water of the eyeball, and normal intraocular pressure is from 11 mmHg to 21 mmHg. In order to ensure the effectiveness of the simulation, intraocular pressure is imitated by imposing uniform pressure on the inner wall of the eyeball, and the pressure value is 17.5 mmHg [24]. In addition, in order to improve the computational efficiency, it is assumed that the cornea is an isotropic symmetric structure on the basis of not affecting the simulation result [16]. The trephine is set as rigid body.

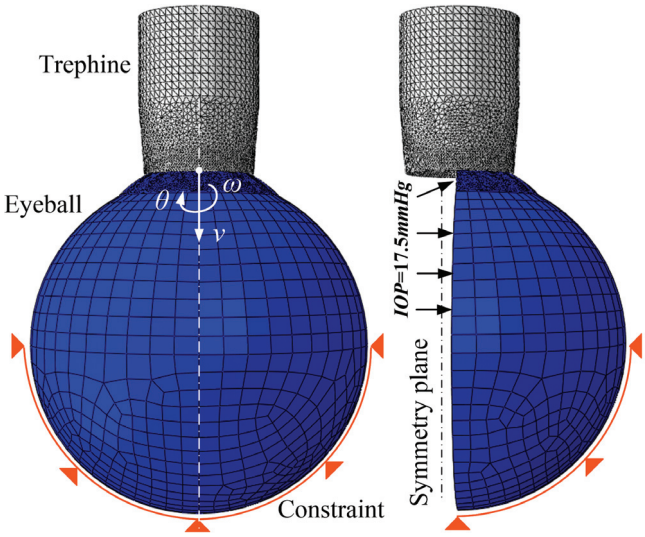

Fig. 2. Three-dimensional finite element model of cutting cornea with trephine

In the eyeball model, the lower hemisphere is hinged, and the vertical motion load v is applied on the center axis of the trephine, and the rotational motion load is applied at the same time including rotation velocity ω and rotation angle θ. In order to describe the rotational motion under the constraint condition, a periodic curve function is established. The function is expressed by Fourier series,

$$a(t) = A_0 = A_0 + \sum_{n=1}^{N} [A_n \cos n\varepsilon(t - t_0) + B_n \sin \varepsilon(t - t_0)] \tag{1}$$

where ε is the circular frequency, and t_0 is the starting time, and A_0 is the initial amplitude, and A_n and B_n

are cosine and sine coefficients. Setting $N = 1$, $B_n = \theta$, $\varepsilon = \omega$ and other parameters are 0. The dynamic explicit analysis step is set in the analysis, and the target time increment is 1.0×10^{-5} s.

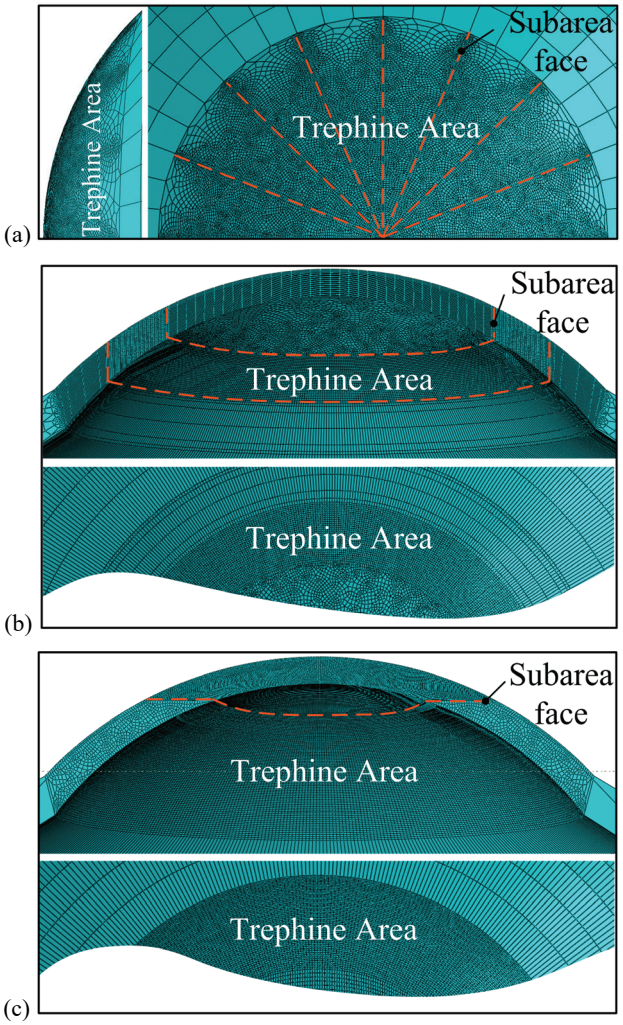

Fig. 3. The mesh of corneal model. (a) umbrella mesh, (b) vertical mesh; (c) horizontal mesh

Because the cornea is thin and irregular, in order to change and simplify the topology, three meshes have been examined based on mesh partition method, as shown in Fig. 3, including the umbrella mesh, the vertical mesh, and the horizontal mesh. As shown in Table 1, the simulation results show that the umbrella mesh can obtain better convergence, with the simulation time of about 68 *s*, and in variation trends and data areas, trephine force has better similarity with the experimental results. Contact algorithm is surface-to-surface contact, in which a rigid material is chosen as the principal surface to obtain the best contact simulation, and the subordinate surface based on node are selected. So, the first contact surface is the trephine, and the second contact surface is the cornea, i.e., the subdivision region in the Fig. 3a. The contact action is tangential contact friction, and the normal pressure is hard contact.

2.2. The three-dimensional failure criterion of cornea material

In order to establish the strength conditions in complex stress states, the researchers have proposed the assumption and calculation method for the failure of materials under various stress conditions, i.e., strength theory. The yield or fracture failure of a material is caused by a factor in stress, strain or strain energy density, and independent of the stress state. Strength theory can also be divided into fracture strength theory of brittle material and yield strength theory of plastic material. In the yield strength theory including the third strength theory and the fourth strength theory, a failure criterion is defined, and the unit loses the load-carrying capacity and is deleted when it meets the failure criterion. The equivalent stress failure criterion, based on the fourth strength theory, is one of the commonly used failure criteria, and is commonly used in small strain polymeric materials [24], [30].

As a typical biomaterial, cornea has hyperelasticity and viscoelasticity. A three-dimensional failure criterion of cornea material have been studied to propose for interaction simulation of trephine with corneal tissue based on the yield strength theory. According to the model of corneal trephination, there are three-dimensional features in the operation, and the material deformation gradient tensor of the cornea, i.e., the stretching tensor F, contains 9 compo-

Table 1. The comparison about different meshes of corneal model

Mesh partition method	Number of meshes		Simulation time [s]	Trephine force compared with experimental data	
	total	trephine area		variation trend	data area
The umbrella mesh	17215	13008	68	similar	similar
The vertical mesh	21064	11709	165	similar	smaller
The horizontal mesh	19377	15560	283	difference	larger

nents in the three-dimensional state, so it can be described as

$$\mathbf{F}=\begin{bmatrix} F_{11} & F_{12} & F_{13} \\ F_{21} & F_{22} & F_{23} \\ F_{31} & F_{32} & F_{33} \end{bmatrix} \tag{2}$$

For symmetric tensors, F_{11}, F_{22}, F_{33} are direct variables, and F_{12}, F_{13}, F_{21}, F_{23}, F_{32}, F_{31} are indirect variables, and $F_{21} = F_{12}$, $F_{32} = F_{23}$, and $F_{13} = F_{31}$. The Mooney–Rivlin constitutive model of corneal material can be described as [23]

$$W=W(\bar{I}_1,\bar{I}_2,J)=C_{10}(\bar{I}_1-3)+C_{01}(\bar{I}_2-3)+\frac{1}{D}(J-1)^2 \tag{3}$$

In the above formula, the volume ratio $J = \det(F)$. $\bar{I}_1$ and $\bar{I}_2$ are the first and second invariants of the symmetric modified Cauchy–Green tensor [7], wherein $\bar{I}_1 = J^{-\frac{2}{3}}I_1$, $\bar{I}_2 = J^{-\frac{4}{3}}I_2$.

Hyperelastic material is characterized by the presence of a potential strain function W, and it is the potential energy of second Piola–Kirchhoff stress tensor **S**, which exists in

$$S=2\left(\frac{\partial W}{\partial \bar{I}_1}\frac{\partial \bar{I}_1}{\partial C}+\frac{\partial W}{\partial \bar{I}_2}\frac{\partial \bar{I}_2}{\partial C}+\frac{\partial W}{\partial J}\frac{\partial J}{\partial C}\right) \tag{4}$$

In the formula, the right Cauchy–Green deformation tensor $\mathbf{C} = \mathbf{F}^T\mathbf{F}$. Through the derivation, the expression of Piola–Kirchhoff stress tensor can be obtained, which is

$$\mathbf{S}=2C_{10}J^{-\frac{2}{3}}\left(\mathbf{I}-\frac{1}{3}I_1C^{-1}\right)+2C_{01}J^{-\frac{4}{3}}\left(\frac{4}{3}I_1\mathbf{I}-\frac{1}{3}I_1I_1C^{-1}-C\right)+\frac{2}{D}(J-1)JC^{-1} \tag{5}$$

where **I** is Unit matrix. Cauchy stress component is described by the Cauchy–Green strain tensor, and there is

$$\boldsymbol{\sigma}=\frac{1}{J}\mathbf{F}\mathbf{S}\mathbf{F}^T=\frac{2}{J}C_{10}\left(\overline{\mathbf{B}}-\frac{1}{3}\mathbf{T}\mathbf{I}\right)+\frac{2}{J}C_{01}\left(\frac{4}{3}\overline{\mathbf{B}}\mathbf{T}-\frac{1}{3}\mathbf{T}\mathbf{T}\mathbf{I}-\overline{\mathbf{B}}\overline{\mathbf{B}}\right)+\frac{2}{D}(J-1)\mathbf{I} \tag{6}$$

In the formula, **T** is the trace of the right Cauchy–Green deformation tensor matrix, i.e., $\mathbf{T} = \text{trace}(\bar{B})$. The corrected right Cauchy–Green deformation tensor $\overline{\mathbf{B}} = \overline{\mathbf{F}}^T\overline{\mathbf{F}}$, in which the modified deformation gradient can be described as $\overline{\mathbf{F}} = J^{-\frac{1}{3}}\mathbf{F}$. In three-dimensional state, $\boldsymbol{\sigma}$ is the 3 × 3 order matrix, that is,

$$\boldsymbol{\sigma}=\begin{bmatrix} \sigma_{11} & \sigma_{12} & \sigma_{13} \\ \sigma_{21} & \sigma_{22} & \sigma_{23} \\ \sigma_{31} & \sigma_{32} & \sigma_{33} \end{bmatrix} \tag{7}$$

where σ_{11}, σ_{22}, σ_{33} are normal stress components, and σ_{12}, σ_{13}, σ_{21}, σ_{23}, σ_{31}, σ_{32} are shear stress components, and $\sigma_{21} = \sigma_{12}$, $\sigma_{32} = \sigma_{23}$ and $\sigma_{13} = \sigma_{31}$.

By calculating the Cauchy–Green stress invariants, the existence of normal stress σ_h and shear stress σ_t can be expressed as

$$\sigma_h=\frac{I_1}{3},\qquad \sigma_t=\frac{1}{3}\sqrt{2+(I_1^2-3I_1)} \tag{8}$$

Based on the static equilibrium equations, σ_h and σ_t can be indicated by stress components, i.e.,

$$\sigma_h=\frac{\sigma_{11}+\sigma_{22}+\sigma_{33}}{3},\qquad \sigma_t=\frac{1}{3}\sqrt{(\sigma_{11}-\sigma_{22})^2+(\sigma_{22}-\sigma_{33})^2+(\sigma_{33}-\sigma_{11})^2+6(\sigma_{12}^2+\sigma_{23}^2+\sigma_{31}^2)} \tag{9}$$

In the above formula, the σ_{11}, σ_{22}, σ_{33}, σ_{12}, σ_{23} and σ_{31} are six stress components in the three-dimensional state. The equivalent stress can be determined by any stress state directly, and by combining (8) and (9), the following formula can be obtained, which is

$$\sigma_s=\sqrt{\frac{1}{2}[(\sigma_{11}-\sigma_{22})^2+(\sigma_{22}-\sigma_{33})^2+(\sigma_{33}-\sigma_{11})^2]+3(\sigma_{12}^2+\sigma_{23}^2+\sigma_{31}^2)} \tag{10}$$

The energy stored due to deformation of an elastic body under the action of applied forces is called strain energy, and the energy stored in a unit volume is called strain energy density. According to the fourth strength theory, the strain energy density is the major factor causing the destruction of materials. No matter what the stress state of the material, the material will yield failure as long as the distortion energy density ρ_d reaches its limit value ρ_{d0}. ρ_{d0} can be determined by the uniaxial tensile test.

$$\rho_{d0} = \frac{2(1+\mu)}{6E}([\sigma])^2 \tag{11}$$

In the above-mentioned formula, $[\sigma]$ is the ultimate stress obtained by the axial tensile test, so the yield limit of the material can be indicated as

$$\rho_d = \rho_{d0} \tag{12}$$

Define the state variable as δ, and the yield failure condition can be expressed as

$$\delta = \sigma_s \leq [\sigma] \tag{13}$$

The formula (13) is the yield condition of the cornea under three-dimensional conditions. Based on the condition, the failure criterion of corneal material is defined and described in the subroutine *VUMAT* of *ABAQUS*. On the basis of the known strain increment, the stress increment of the material is obtained, and the equivalent stress of the material is calculated. When the unit of the material meets the defined failure criterion in simulation, it loses the carrying capacity and is removed from the model. The state variable δ is defined as a constant before being compared with the limit stress $[\sigma]$. In calculations, if $\delta < [\sigma]$, the state variable δ is defined as 0, which means that the material failure, otherwise, $\delta = 1$ means that the material is normal. In integral point of material of each time step, the main program will call the subroutine for failure calculation. Then, in the next time step, if the initial state variable $\delta_0 \neq 0$, the program will continue to perform the operation, and the judgement of the material failure is proceeded.

Problems occuring in the numerical simulation of corneal trephination, are great deformation and changing contact surface, besides the failure and destruction of the corneal structure layer. At present, an explicit solver can be used to deal with this kind of problem [8], and the material failure and separation can be achieved using the unit deletion technology.

3. Results

The process of corneal trephination involves the instantaneous three-dimensional status of the interaction between rigid body and soft tissue, and it is more complex and difficult to calculate, compared to the simulation of needle insertion into soft tissue. Based on the established numerical model of corneal trephination and the three-dimensional failure criterion of corneal material, the numerical simulation of trephine cutting cornea is carried out, and the changes of trephine forces are discussed. Comparison of the results of corneal trephination, which is operated by robots with the same parameters is made and the validity of the simulation is verified.

The simulation parameters are set as $[v, \theta, \omega] = [20.0, 1.25, 33.5]$, where v is the velocity of the vertical motion and the unit is μm/s, θ is the angle of the rotary motion and the unit is *rad*, ω is the angular velocity of the rotary motion and the unit is *r*/min (i.e., revolutions per minute). The simulation is carried out in *ABAQUS*, where simulation time is 70 s, and the change curves of trephine forces with displacement are shown in Fig. 4. Figure 4a describes rotating load in the simulation, and the peak value, *A* point, shows the rotation angle $\theta = 1.25$ *rad*. Figures 4b and 4c, present the change curves of the linear cutting force F_z and the rotary cutting force F_c, respectively. In the figures, the *AB* interval is the effective interval for trephination simulation, and the simulation time is about 60 s. In Fig. 4b, the curve *a* is the sampling data, and the curve *b* is the fitting curve obtained by fitting the sampling data by Gauss interpolation, and the fitting function $g(x)$ is shown in the formula (14). The curve *a* shows a fluctuation growth and the stability can be improved by changing the precision of mesh division and the setting of time increment step. At point *C*, the linear cutting force F_z reaches the maximum value which is 14.40×10^{-2} *N*, and the puncture force F_p is about 2.76×10^{-2} *N*. The epithelium has been punctured at point *D*, and point *E* shows the corresponding linear cutting force at the time of 38.5 s. From the fitting curve *b*, the change regulation of the linear cutting force F_z can be shown, and it shows an obvious decline when the stroma has been punctured at point *B*. In Fig. 4c, rotating cutting force F_c shows a periodic change and an obvious increasing trend, and the maximum value of the force F_c is about 3.55×10^{-2} *N*. After a stable state, the force F_c reaches the punctured position, i.e., point *B*, and it shows the reducing trend, periodic

variation and kept constant. The fitting function of sampled data is

$$g(x)=\sum_{i=1}^{2} a_i \exp\left(-\left(\frac{x-b_i}{c_i}\right)^2\right) \quad x\in[0,70] \qquad (14)$$

in which,

$$\begin{bmatrix} a_1 & b_1 & c_1 \\ a_2 & b_2 & c_2 \end{bmatrix} = \begin{bmatrix} 0.10 & 62.36 & 22.04 \\ 0.06 & 33.86 & 18.63 \end{bmatrix}.$$

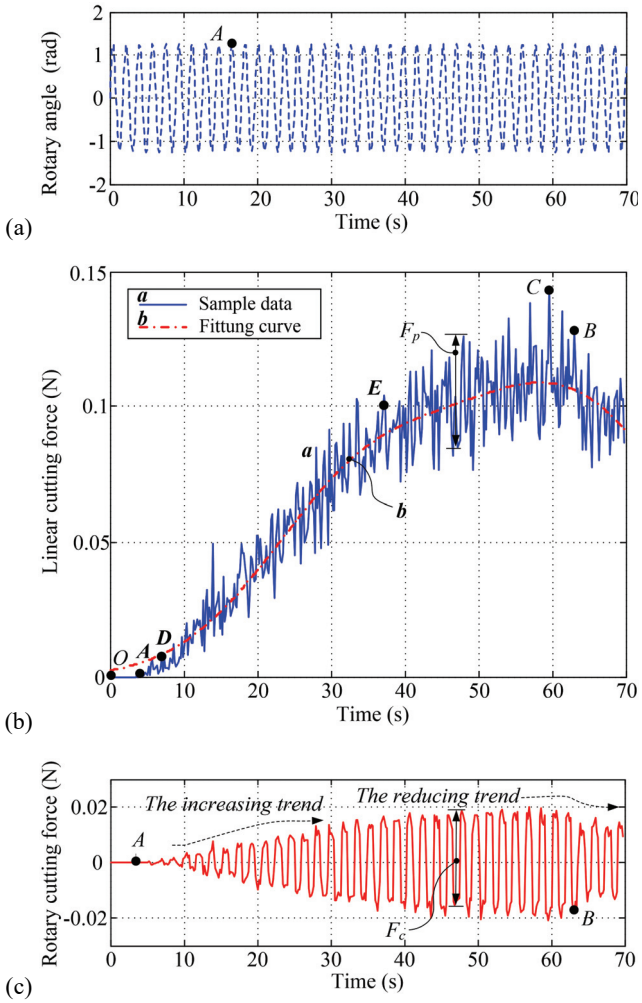

Fig. 4. Simulation results of trephination.
(a) the relationship between time and rotary angle,
(b) simulation curves of the linear cutting force,
(c) simulation result of rotary cutting force

The equivalent stress maps of trephination simulation are shown in Fig. 5, which reflects the destruction and deformation of the cornea in the process of trephination. Figures 5a–e correspond to the points *O*, *A*, *D*, *E*, and *B* of Fig. 4, respectively. Figure 5a depicts the initial state of the simulation. Figure 5b shows that the trephine contacts and extrudes the corneal surface when the simulation time is about 3.5 s, and the obvious stress changes are shown in the whole cornea due to extrusion force and intraocular pressure. Figure 5c shows that the epithelium has been punctured when the simulation time is about 7.7 s, and due to the failure stress and material are different, the two cell layers can be clearly identified from the figure. Figure 5d shows the deformation and destruction of the cornea when the simulation time is about 38.5 s. The shade is the initial state of the simulation, and the entity is the instantaneous state of trephination. By comparing two statues, it can be shown that the whole cornea and the unconstrained sclera will have occurred apparent elastic deformation in the process. Figure 5e shows the equivalent stress state where the stroma has been punctured when the simulation time is about 62.5 s, and it can be regarded that the whole cornea was completely punctured, and the deformation of the cornea is marked as *m*. Figure 5f is the stress state when the cornea is penetrated and the simulation time is about 65 s, and it can be seen that the current state of corneal deformation marked as *n* is more apparent than the deformation *m* in Fig. 5e. It illustrates that the cornea is affected by the intraocular pressure after it has been punctured in the simulation, and will also produce reaction force to the trephine, so the trephine force will not disappear immediately, which is consistent with the analysis of the trephine force above.

In order to verify the simulation, the experiment of robotic trephination is carried out [22], as shown in Fig. 6, where the operating parameters are set up with reference to the simulation parameters. The experiment results of robotic trephination are obtained, as shown in Fig. 7. In Fig. 7a, the *AB* interval is the effective interval of trephination experiment, and the time is about 90 s, which is longer than the simulation time. That shows that the deformation of the eyeball in the experiment is greater than the simulation. At point *C*, The linear cutting force F_z reached the maximum value of about 14.92×10^{-2} *N*, and the maximum value of the puncture force F_p is about 2.30×10^{-2} *N*. These two values are basically close to the values of the simulation. The trephine force drops rapidly to near the zero point after point *B*, indicating that the cornea has been punctured and has lost carrying capacity of the trephine. In Fig. 7b, the rotary cutting force F_c, which is less than 2.40×10^{-2} *N*, shows an obvious trend of increase, and it is similar to the simulation results. In the simulation and the experiment, the trephine forces are shown in Table 2, where the data correspond to the force curves. Before the

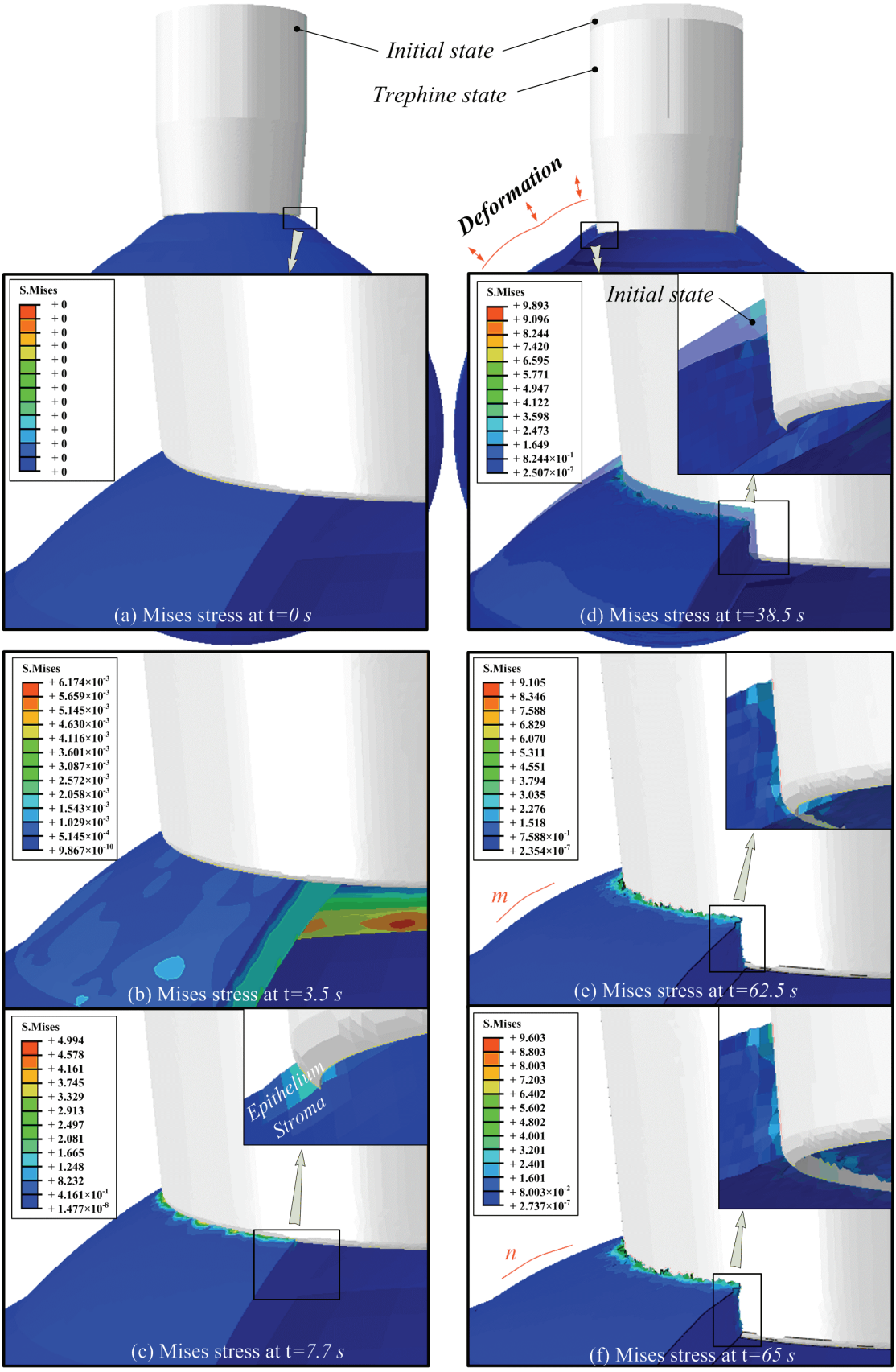

Fig. 5. The equivalent stress maps of trephination simulation, where t is trephination time.
(a) corneal pre-deformed status, (b) cutting status of epithelium at t = 3.5 s, (c) corneal epithelium has been punctured,
(d) cutting status of stroma at t = 38.5 s, (e) the stroma has been punctured,
(f) broken status of the cornea at t = 65 s

cornea is punctured, it shows corneal deformation that the displacements are greater than the corneal thickness. Comparing the results of experiment with that of simulation, it is shown that the change and data area of the trephine forces are in agreement. The modeling and simulation on interaction of trephine with cornea are correct and effective, and the simulation can reflect the biomechanical characteristics of the experiment.

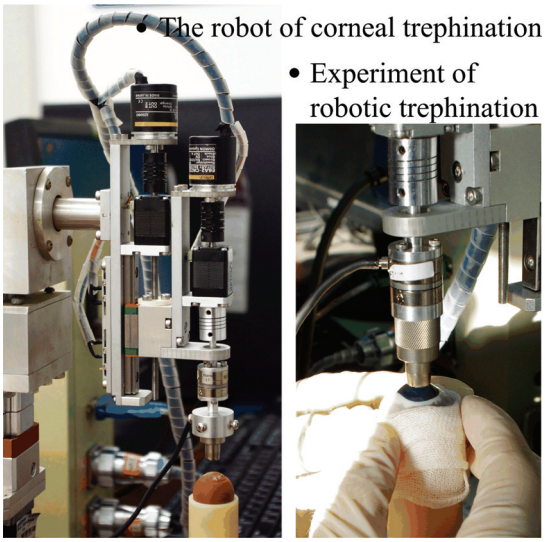

Fig. 6. The experiment of robotic trephination.
(a) the robot of corneal trephination,
b) experiment of robotic thephination

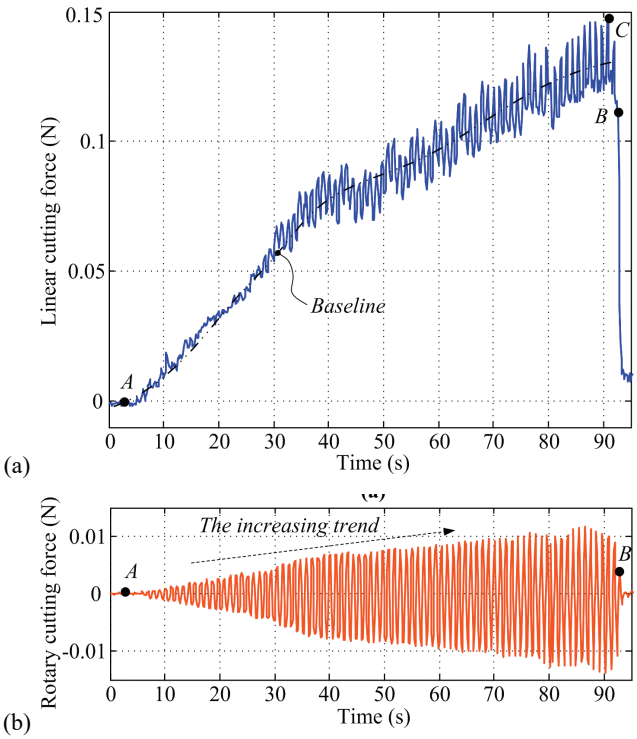

Fig. 7. The experimental results of the robotic trephination.
(a) experimental curves of the linear cutting force,
(b) the result of rotary cutting force

Table 2. Statistics on the trephine forces, where simulation data of the linear cutting force F_z is the fitting value and experimental data of the force F_z is the mean value

Time [s]	Displacement [μm]	Simulation		Experiment	
		F_z (*N*)	F_c (*N*)	F_z (*N*)	F_c (*N*)
0	0	0	0	0	0
3.5	70	0.72	0	0	0.01
7.7	154	0.81	0.16	0.78	0.03
30	600	7.31	2.77	5.70	1.07
38.5	770	8.80	3.43	5.75	1.30
50	1000	10.04	3.55	8.82	1.62
58.1	1162	11.05	3.50	9.05	1.65
62.5	1250	14.40	3.28	10.00	2.12
65	1300	10.78	3.05	10.05	2.31
90.3	1806	9.65	3.12	12.83	2.40
92.5	1850	9.53	3.08	11.21	2.32
95	1900	9.59	3.16	1.31	0.01
100	2000	9.60	3.10	1.06	0.01

4. Discussion

A three-dimensional model of interaction of trephine with corneal tissue is established, and it is a new attempt to confirm that the cornea consists of different structural layers that have different geometric thickness and different mechanical properties. On this basis, the finite element model is established where the mesh of the cornea is refined based on partition method of umbrella mesh that has better performance than vertical or horizontal mesh. Simulation results demonstrate that the umbrella mesh improves the efficiency and convergence of the finite element simulation. In the simulation, the motion of the trephine cutting cornea is defined by a periodic curve function, i.e., Fourier series, and these loads generate the vertical velocity, the rotation velocity and the rotation angle. It simulates the surgeon's operation, including the vertical motion and the rotational motion.

In the research of trephine cutting cornea, it is essential to explore the assumption and calculation method for the failure of materials under mechanics theory. A three-dimensional failure criterion of corneal material is proposed based on the yield strength theory, where the three-dimensional form of the equivalent stress can be evaluated on the basis of mathematic deduction. Based on the criterion, the units of corneal material are removed from the model due to the loss of the carrying capacity when they meet the defined failure criterion. And the results show that the criterion may be used for corneal material within a certain range of accuracy.

By three-dimensional simulation of corneal trephination under determined simulation parameters, the change curves of trephine forces with cutting displacement are obtained during the process. Among them, the linear cutting force continues to increase due to the reaction force caused by squeezing the eyeball. Although the punctured cornea lose the carrying capacity due to the disappearance of constraints in the simulation, the failure unit and the normal unit still give trephine friction force and reaction force in the process of simulation, so the force did not fall to zero position after the cornea has been punctured. The rotary cutting force shows a periodic change and an obvious increasing trend. Then, the equivalent stress maps of the finite element simulation are analyzed, which correspond to the marked points of the trephine forces curves, and they show the failure process of the corneal material.

The experiment of robotic trephination is carried out under the same parameters to verify the simulation. The results show that the simulation results are basically consistent with the experimental results in variation trend and data area of trephine forces, and the simulation can reflect the biomechanical behavior of the operation.

The research has reproduced the process of the interaction of trephine with cornea, and the biomechanical model of corneal trephination is the basis for the surgery simulation and training system based on force feedback. Further studies are necessary to explore the real-time simulation of the surgery based on finite element methods and sensor technology.

Acknowledgements

The author wishes to thank Young Elite Scientists Sponsorship Program by CAST (Grant No. YESS20160065), Training Plan of Young Top-notch Talent by Beijing Municipal Education Commission (Grant No. CIT&TCD201704063), and the Fund of Beijing Key Laboratory for Photoelectric Measurement Technology (Grant No. GDKF2017001) that supported this work.

References

[1] ABOLHASSANI N., PATEL R., MOALLEM M., *Needle insertion into soft tissue: a survey*, Med. Eng. Phys., 2007, 29(4), 413–431.

[2] ALMAMOUN A., *Influence of different keratoplasty techniques on the biomechanical properties of the cornea*, Acta Ophthalmol., 2013, 91(7), e567–572.

[3] ANDERSON K., EL-SHEIKH A., NEWSON T., *Application of structural analysis to the mechanical behaviour of the cornea*, J. R. Soc. Interface, 2004, 1(1), 3–15.

[4] BASSAN H.S., PATEL R.V., MOALLEM M., *A novel manipulator for percutaneous needle insertion: design and experimentation*, IEEE-ASME T. Mech., 2009, 14(6), 746–761.

[5] BOURNE W.M., *Morphologic and functional evaluation of the endothelium of transplanted human corneas*, Trans. Am. Ophthalmol. Soc., 1983, 81, 403–450.

[6] DI-MAIO S.P., SALCUDEAN S.E., *Needle insertion modeling and simulation*, IEEE Trans. Robot. Autom., 2003, 19(5), 864–875.

[7] HOLZAPFEL G.A., *Nonlinear solid mechanics: a continuum approach for engineering*, Meccanica, 2000, 37(4–5), 489–490.

[8] IQBAL M.A., CHAKRABARTI A., BENIWAL S., GUPTA N.K., *3D numerical simulations of sharp nosed projectile impact on ductile targets*, Int. J. Impact. Eng., 2010, 37(2), 185–195.

[9] JAFARINASAB M.R., FEIZI S., JAVADI M.A., HASHEMLOO A., *Graft biomechanical properties after penetrating keratoplasty versus deep anterior lamellar keratoplasty*, Curr. Eye Res., 2011, 36(5), 417–421.

[10] KORFF A., FOLLMANN A., FÜRTJES T., HABOR D., *Concept and evaluation of a synergistic controlled robotic instrument for trepanation in neurosurgery*, Mach. Vision Appl., 2011, 21(2), 163–176.

[11] LIU X., WANG L., WANG C., SUN G., LIU S., FAN Y., *Mechanism of traumatic retinal detachment in blunt impact: a finite element study*, J. Biomech., 2013, 46(7), 1321–1327.

[12] MAJID M., MEYER J.J., KANG P.C., *A comparison of three methods for trephining donor corneal buttons: endothelial cell loss and microscopic ultrastructural evaluation*, Curr. Eye Res., 2009, 34(11), 939–944.

[13] NIELS E., JESPER H., *Corneal thickness: measurement and implications*, Exp. Eye Res., 2004, 78(3), 543–548.

[14] HU Y., LI D., YANG Y., SUN X., *Integration of microsensor for microsurgery robot's end-effector*, J. B. Univ. Aeronaut. Astronaut., 2007, 2(2), 205–209.

[15] HOFFART L., PROUST H., MATONTI F., RIDINGS B., CONRATH J., *Short-term results of penetrating keratoplasty performed with the femtec femtosecond laser*, Am. J. Ophthalmol., 2008, 146(1), 50–55.e1.

[16] PINSKY P.M., HEIDE D.V.D., CHERNYAK D., *Computational modeling of mechanical anisotropy in the cornea and sclera*, J. Cataract. Refr. Surg., 2005, 31(1), 136–145.

[17] RAVALI G., MANIVANNAN M., *Haptic feedback in needle insertion modeling and simulation: review*, IEEE Rev. Biomed. Eng., 2017, pp(99), 1–1.

[18] ROBERTS C., *The cornea is not a piece of plastic*, J. Refract. Surg., 2000, 16(4), 407.

[19] SOONG H.K, MALTA J.B., *Femtosecond lasers in ophthfalmology*, Am. J. Ophthalmol., 2009, 147(2), 189–197.e2.

[20] STUDER H., LARREA X., RIEDWYL H., BÜCHLER P., *Biomechanical model of human cornea based on stromal microstructure*, J. Biomech., 2009, 43(5), 836–842.

[21] STUDER H.P., RIEDWYL H., AMSTUTZ C.A., HANSON J.V.M., BÜCHLER P., *Patient-specific finite-element simulation of the human cornea: a clinical validation study on cataract surgery*, J. Biomech., 2012, 46(16), 751–758.

[22] SU P., DENG S., HUANG L., SONG Y., LIU X., YANG Y., *Analysis and evaluation of a robotic trephination in penetrating keratoplasty*, J. Med. Devices, 2016, 10(2).

[23] SU P., YANG Y., XIAO J., SONG Y., *Corneal hyperviscoelastic model: derivations, experiments, and simulations*, Acta Bioeng. Biomech., 2015, 17(2), 73–84.

[24] SU P., YANG Y., ZHANG L., HUANG L., *Biomechanical simulation of needle insertion into cornea based on distortion energy failure criterion*, Acta Bioeng. Biomech., 2016, 18(1), 65–75.

[25] SZENTMÁRY N., LANGENBUCHER A., KUS M.M., NAUMANN G.O., SEITZ B., *Elliptical nonmechanical corneal trephination: intra-*

operative complications and long-term outcome of 42 consecutive excimer laser penetrating keratoplasties, Cornea, 2007, 26(4), 414–420.

[26] TAYLOR R., DU X., PROOPS D., REID A., COULSON C., BRETT P.N., *A sensory-guided surgical micro-drill*, Archive P. I. Mech. Eng. G.-J. Aer. 1989–1996 (Vols. 203–210), 2010, 224(7), 1531–1537.

[27] TAYLOR R.H., STOIANOVICI D., *Medical robotics in computer-integrated surgery*, IEEE Trans. Rob. Autom., 2003, 19(5), 765–781.

[28] YANG Y.F., CHEN D.F., ZENG Y.J., ZHANG B., *Simulation of corneal tissue mechanical deformation based on the finite element method*, J. B. Univ. Technol., 2008, 34(1), 85–89.

[29] YANG Y., XU C., DENG S., XIAO J., *Insertion force in manual and robotic corneal suturing*, Int. J. Med. Robot. Comp., 2012, 8(1), 25–33.

[30] YAN J., STRENKOWSKI J.S., *A finite element analysis of orthogonal rubber cutting*, J. Mater. Process. Tech., 2006, 174(1), 102–108.